Bioorganic & Medicinal Chemistry xxx (xxxx) xxxx

Contents lists available at ScienceDirect

Bioorganic & Medicinal Chemistry

journal homepage: www.elsevier.com/locate/bmc

3D proteome-wide scale screening and activity evaluation of a new ALKBH5 inhibitor in U87 glioblastoma cell line

Alessio Malacrida[b,1], Mirko Rivara[a,*,1], Alessandro Di Domizio[c,d], Giacomo Cislaghi[d], Mariarosaria Miloso[b], Valentina Zuliani[a], Gabriella Nicolini[b]

[a] Food and Drug Department, University of Parma, Parco Area delle Scienze 27/A, 43124 Parma, PR, Italy
[b] School of Medicine and Surgery, Experimental Neurology Unit and Milan Center for Neuroscience, University of Milano-Bicocca, via Cadore 48, 20900 Monza, MB, Italy
[c] Department of Pharmacological and Biomolecular Sciences, University of Milano, via Balzaretti 9, 20133 Milano, Italy
[d] SPILLOproject, via Stradivari 17, 20037 Paderno Dugnano, Milano, Italy[2]

ARTICLE INFO

Keywords:
Glioblastoma
ALKBH5
Imidazobenzoxazin-5-thione scaffold
Off-target interaction

ABSTRACT

The imidazobenzoxazin-5-thione MV1035, synthesized as a new sodium channel blocker, has been tested on tumoral cells that differ for origin and for expressed Na_V pool (U87-MG, H460 and A549). In this paper we focus on the effect of MV1035 in reducing U87 glioblastoma cell line migration and invasiveness. Since the effect of this compound on U87-MG cells seemed not dependent on its sodium channel blocking capability, alternative off-target interaction for MV1035 have been identified using SPILLO-PBSS software. This software performs a structure-based *in silico* screening on a proteome-wide scale, that allows to identify off-target interactions. Among the top-ranked off-targets of MV1035, we focused on the RNA demethylase ALKBH5 enzyme, known for playing a key role in cancer. In order to prove the effect of MV1035 on ALKBH5 *in vitro* coincubation of MV1035 and ALKBH5 has been performed demonstrating a consequent increase of N6-methyladenosine (m6A) RNA. To further validate the pathway involving ALKBH5 inhibition by MV1035 in U87-MG reduced migration and invasiveness, we evaluated CD73 as possible downstream protein. CD73 is an extrinsic protein involved in the generation of adenosine and is overexpressed in several tumors including glioblastoma. We have demonstrated that treating U87-MG with MV1035, CD73 protein expression was reduced without altering CD73 transcription. Our results show that MV1035 is able to significantly reduce U87 cell line migration and invasiveness inhibiting ALKBH5, an RNA demethylase that can be considered an interesting target in fighting glioblastoma aggressiveness. Our data encourage to further investigate the MV1035 inhibitory effect on glioblastoma.

1. Introduction

Glioblastoma (GBM, grade IV glioma) represents the most aggressive brain neoplasm and patients with GBM have a poor prognosis. Despite various combinations of surgery, chemotherapy and radiotherapy, GBM is characterized by frequent recurrence and very high lethality. In fact, patients with GBM show a median survival of only 15 months after diagnosis.[1] The greatest challenge in developing a therapy able to arrest GBM invasiveness is represented by glioblastoma stem cells (GSCs) that are very heterogeneous and are responsible for GBM chemoresistance and radio resistance as well as for the ability of GBM to infiltrate neighbouring healthy brain tissue. Moreover drug delivery to GBM is difficult due to the complex structure of the blood brain tumor barrier (BBTB).[2–4] Until now surgical resection followed by radiotherapy and temozolomide (TMZ) treatment represent the standard strategy for GBM.[5,6] However almost all patients manifest resistance and are subject to relapses more aggressive than the primary tumors.[1]

Among the various strategies that could be followed to limit the aggressiveness of GBM, we figured out if targeting sodium channels could have been a suitable approach. Our hypothesis was based on the fact that several studies reported the role of Voltage-Gated Sodium Channels (VGSCs or Na_V) in cancer cells, where they seem associated with cell migration and invasiveness.[7–9]

Abbreviations: DMSO, dimethyl sulfoxide; RT-PCR, reverse transcription polymerase chain reaction; TTX, tetrodotoxin

* Corresponding author at: Food and Drug Department, University of Parma, Parco Area delle Scienze 27/A, 43124 Parma, PR, Italy.
E-mail address: mirko.rivara@unipr.it (M. Rivara).

[1] Alessio Malacrida and Mirko Rivara equally contributed.

[2] Website: www.spilloproject.com.

https://doi.org/10.1016/j.bmc.2019.115300
Received 24 September 2019; Received in revised form 18 December 2019; Accepted 26 December 2019

In particular Na_V are macromolecular protein complexes that are present in both excitable and non-excitable cells. They are involved in the generation of action potential, but also in different physiological processes.[10–12]

Moreover, Na_V are widely expressed in various cancers, including small-cell lung cancer, non-small-cell lung cancer, prostate cancer, melanoma, breast cancer, neuroblastoma, mesothelioma, cervical cancer, ovarian cancer and gliomas.[13–18]

Literature data bring evidence regarding the implication of ion channels in GBM.[19–21] Since $Na_V1.1$, $Na_V1.2$, $Na_V1.3$ and $Na_V1.6$ are the isoforms mainly expressed in the CNS,[22] we have investigated the effects of some sodium channel blockers, previously synthesized by us, with a documented blocking capability against Na_V, on GBM cell proliferation, migration and invasion.

Among the compounds tested (data not shown) the 2-methyl-3-propyl-5H-imidazo[1,2-c][1,3]benzoxazin-5-thione (MV1035)[23] showed a peculiar activity on glioblastoma cells that, unexpectedly, seemed not related with the sodium channel blockade (see results). In order to identify a molecular mechanism able to justify MV1035 effect we used *SPILLO potential binding sites searcher* (SPILLO-PBSS)[24,25] to perform an *in silico* screening of the human structural proteome publicly available in the RCSB Protein Data Bank.[26,27] SPILLO-PBSS is an innovative software designed to identify target proteins of any small molecule on a proteome-wide scale. Their putative binding sites are successfully recognized even within really strongly distorted protein conformations.[24,25]

Among the top-ranked potential targets for MV1035 provided by the *in silico* analysis, we focused our attention on the RNA demethylase ALKBH5 (α-ketoglutarate-dependent dioxygenase alkB homolog 5), which catalyses the conversion of N6-methyladenosine (m6A) to adenosine in mRNA, in the presence of 2-oxoglutarate, molecular oxygen, and iron(II).[28] It is widely demonstrated that m6A RNA methylation represents a post transcriptional modification crucial for modulating expression of proteins involved in tumor initiation and progression.[29] Interestingly, Zhang et al. have demonstrated that ALKBH5 is overexpressed in glioblastoma stem-like cells (GSCs) being fundamental to maintain GSCs tumorigenicity. Moreover investigating the ALKBH5 target mRNA, they have identified the gene encoding for CD73.[30]

Ecto-5′-nucleotidase (ecto-5′-NT, NT5E or CD73) is an extrinsic protein linked to the extracellular surface of the plasma membrane through glycosylphosphatidylinositol (GPI). Besides its enzymatic activity CD73 acts as adhesive and signalling molecule influencing invasiveness and metastatic properties of cancer cells.[31] Furthermore it has been demonstrated that extracellular adenosine influences glioma proliferation[32] and CD73 promotes glioma cell line growth.[33,34]

Here we show, integrating cellular, molecular and *in silico* techniques, that MV1035 reduces GBM cell line U87 migration and invasiveness, targeting the SPILLO-PBSS recognized RNA N6-methyladenosine (m6A) demethylase ALKBH5 activity and ultimately inducing a decrease in CD73 expression.

2. Material and methods

2.1. Biological evaluation

2.1.1. Cell lines

The choice of cell lines was based on the expression of Nav: U87-MG and H460 cells express functionally active Nav, on the contrary A549 cells lack functional Nav.

A549 (ATCC® CCL-185™) and H460 (ATCC® HTB-177™) human non-small lung cancer cell lines were cultured in RPMI 1640 medium supplemented with 10% Fetal Bovine Serum (FBS), 1% L-Glutamine and 1% Penicillin/Streptomycin (Euroclone, Italy). U87-MG glioblastoma cell line U87-MG (ATCC® HTB14™) was cultured in DMEM-Low Glucose medium supplemented with 10% Fetal Bovine Serum (FBS), 1% L-Glutamine and 1% Penicillin/Streptomycin (Euroclone, Italy). Cells were incubated at 37 °C and 5% CO2 in a humidified incubator.

MV1035 was solubilized (10 mM) in DMSO and then it was diluted directly into culture medium to working concentrations.

2.1.2. MTT assay

Cells were seeded in 96-well plates at a density of 10^4 cells/well. After 24 h, cells were treated for further 24 h with increasing concentrations of MV1035, tetrodotoxin (TTX) or EN300. At the end of the treatment, cells were washed with PBS Ca^{++}/Mg^{++} and a solution of MTT 0.5 mg/ml in DMEM without phenol red was added (Sigma Aldrich, USA). After 2 h of incubation at 37 °C, cells were washed with PBS Ca^{++}/Mg^{++} and MTT formazan salt was solubilized with 100% ethanol. Optical density of the MTT solution was measured using a multiplate reader at a 570 nm wavelength (BMG Labtech, Germany).

2.1.3. SRB assay

Cells were seeded and treated as described in MTT assay section. After 24 h of treatment, cells were fixed with trichloroacetic acid for 1 h at 4 °C. Cells were then washed with tap water and stained with Sulforhodamine B (SRB) solution. After washing with 1% acetic acid, SRB was solubilized with 10 mM Tris(Hydroxymethyl)aminomethane. The optical density of the solution was quantified using a multiplate reader at a 540 nm wavelength (BMG Labtech, Germany).

2.1.4. Scratch wound healing assay

Cells were seeded in 6-well plates at high density. When cells reached a confluence of 90–100%, complete culture medium was replaced with serum-free medium. After 24 h, a scratch was made on cell monolayer using a plastic tip. Wells were washed with PBS to remove detached cells and debris and complete culture medium, with or without MV1035, TTX or EN300, was added. Micrographs were taken immediately after the scratch and after 6 h (U87-MG) or 24 h (A549 and H460). Different time points (6 or 24 h) have been decided considering different cell lines migration capacity. Cell migration area was measured using ImageJ software.

2.1.5. Boyden chamber assay

The lower compartments of the Boyden chamber were filled with complete culture medium (with 10% FBS used as chemoattractant). In the upper compartment of the Boyden chamber, cells resuspended in serum-free medium, with or without MV1035, TTX or EN300, were placed at a density of 10^4 cells/well. A gelatine coated polycarbonate membrane with 8 μm pores was placed between the two compartments (Biomap, Italy).

After 24 h of incubation at 37 °C, the membrane was removed and cells on the upper side of the membrane were removed with a plastic blade. Cells on the lower surface of the membrane were fixed with methanol and stained with DiffQuick staining solution (Biomap, Italy). Micrographs were taken under a light microscope and the number of cells that go through the membrane were counted using ImageJ software.

2.1.6. Western blotting

Cells were seeded in 6-well plates at density of $2.5x10^5$ cells/well and treated with MV1035. After 1, 2, 4, 6 and 24 h of treatment total protein extracts were obtained using lysis buffer (50 mM Hepes pH 7.5, 150 mM NaCl, 10% glycerol, 1% Triton X100, 1.5 mM $MgCl_2$, 5 mM EGTA, 4 mM PMSF, 1% Aprotinin, 10 mM sodium orthovanadate and 20 mM sodium pyrophosphate) and mechanical scraping. Protein solution was clarified with a centrifuge at 18,000*g* for 15 min at 4 °C and protein content was quantified using Bradford method. Proteins were then loaded in SDS-page polyacrylamide gel after chemical and thermal denaturation. After electrophoresis, proteins were transferred to nitrocellulose filters and immunoblotting analysis was performed following manufacturer instructions. Briefly, antibodies against CD73 (1:1000, BD biosciences, USA) and beta actin (1:1000, Santa Cruz Biotechnology, USA) were used. After incubation with primary

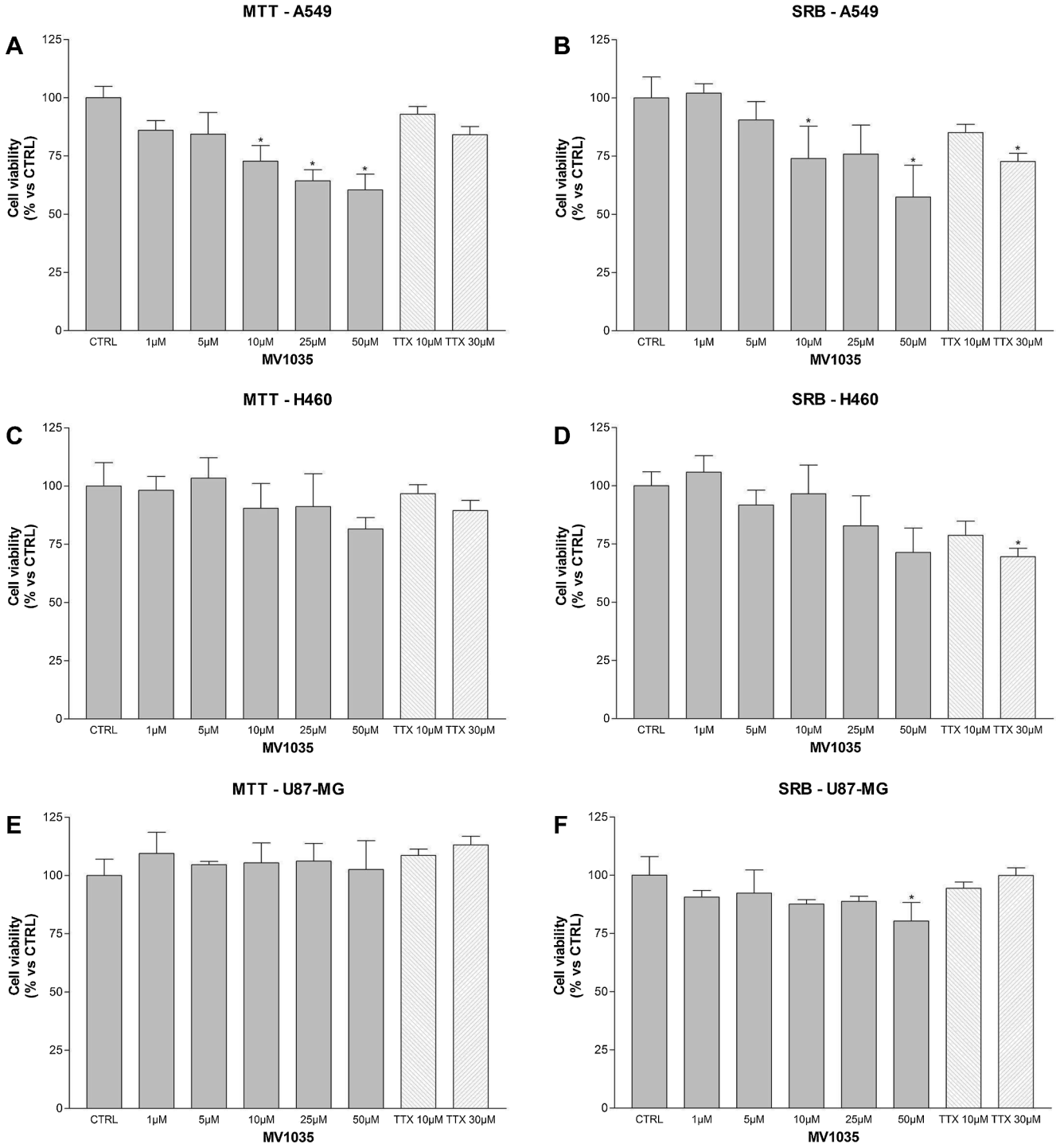

Fig. 1. MV1035 effect on cell viability of A549, H460 and U87-MG. MTT and SRB assay of A549 (A and B), H460 (C and D) and U87-MG (E and F) cells treated with increasing concentrations of MV1035 (1–50 μM) and TTX (10–30 μM). Graphs represent the average percentage ± SD of viable cells of three independent experiments compared to untreated control cells (CTRL, 100%) (* $p < 0.05$ vs CTRL).

antibodies, membrane was washed and then incubated with appropriate horseradish peroxidase-conjugated secondary antibodies (1:2000) (anti-mouse, Chemicon, USA; anti-rabbit, PerkinElmer, USA). Immunoreactive proteins were visualized using an ECL chemiluminescence system (Amersham, USA).

2.1.7. RNA demethylation assay

4 μM active recombinant ALKBH5 protein (Active Motif), 80 μM M6A-ssRNA (sequence GG-m6A-CU) (Ella Biotech, Germany), 150 μM α-ketoglutarate, 150 μM ammonium iron sulphate hexahydrate, 2 mM L-ascorbate, 50 mM Hepes pH 7.5 (Sigma Aldrich, USA) were mixed in a microtube and incubated at 4 °C for 30 min. The reaction was stopped by adding 20% formic acid (Sigma Aldrich, USA). 2 μl of reaction solution were placed on a nitrocellulose membrane and a dot blot against m6A-RNA was performed following manufacturer's instructions. Primary antibody against m6A-RNA (1:250, Sigma Aldrich, USA) and secondary antibody anti mouse (1:2000, Jackson Immuno Research, UK) were used.

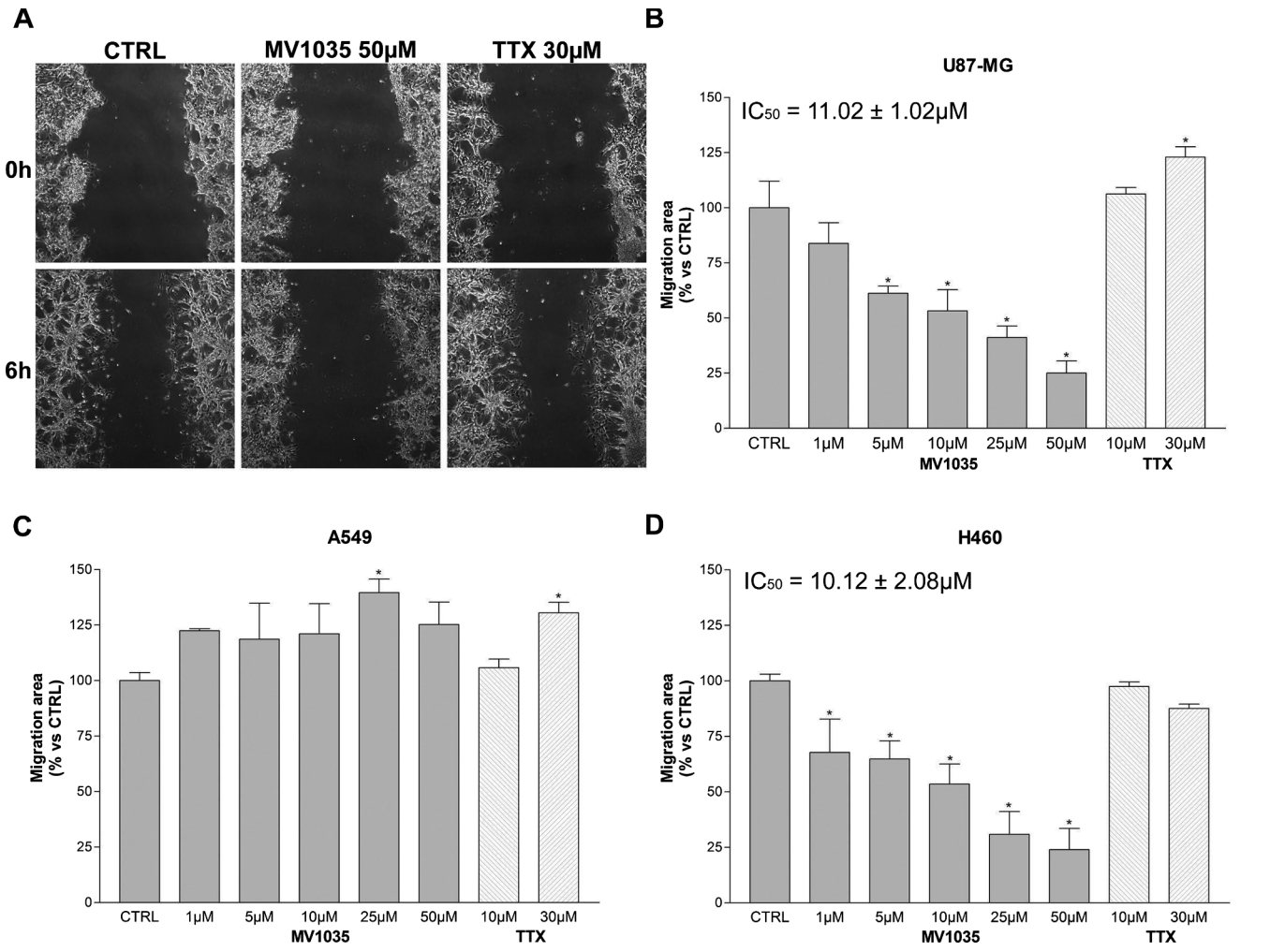

Fig. 2. Migration of cells treated with MV1035 and TTX – Representative images of scratch wound healing assay of U87-MG cells not-treated (CTRL) or treated with MV1035 50 μM or TTX 30 μM, after 0 and 6 h (A). Graphs represent U87-MG (B), A549 (C) and H460 (D) cell migration quantification after treatment with increasing concentrations of MV1035 (1–50 μM) or TTX (10–30 μM). Data are represented as the average percentage ± SD of three independent experiments compared to untreated controls (CTRL, 100%) (* $P < 0.05$ vs CTRL).

2.1.8. RT-PCR

Cells were seeded and treated as described in western blotting paragraph. Total RNA was isolated from cells with TriPure isolation reagent. The quality of RNA extracts was assessed with spectrophotometer (BMG Labtech, Germany). 1 μg total RNA was reverse transcribed and obtained cDNA was amplified and analysed using specific CD73 primers (Hs 00159686 m1, Thermofisher, USA).

2.1.9. Statistics

Data are reported as the average ± standard deviation (SD) from at least three independent experiments. Statistical analysis was performed using GraphPad Prism 3 software. The differences between control and treated cells were evaluated using One Way ANOVA analysis of variance followed by Dunnett's multiple comparison test. Statistical significance was set at $p < 0.05$.

2.2. Materials and Methods

2.2.1. Protein database preparation

The protein database used for SPILLO-PBSS screening is kept constantly updated as the number of protein 3D-structures publicly available in the Protein Data Bank (PDB)[26] increases. For this work we used a database (update September 2017) that included 14537 human holo- and apo-protein 3D-structures, experimentally solved by either X-ray diffraction or solution NMR, excluding 100% sequence identity redundancies.

Biological assemblies for proteins showing multimeric structures were generated by the MakeMultimer program,[56] according to the BIOMT transformation matrices included into the PDB files. For multi-model PDB files from solution NMR experiments, only the first model was included in the database. No further protein structure refinements were needed to improve the quality of protein structures in the database.

2.2.2. RBS generation

The reference binding site (RBS) used by SPILLO-PBSS to search the proteins of the database for similar potential binding sites (PBSs) for MV1035 included 15 amino acid residues directly interacting with MV1035, without any water mediated contact. It was generated by molecular modelling techniques and the standard RBS generation protocol described in SPILLO-PBSS paper.[24] The full list of amino acid residues included in the RBS, along with their weights representing the

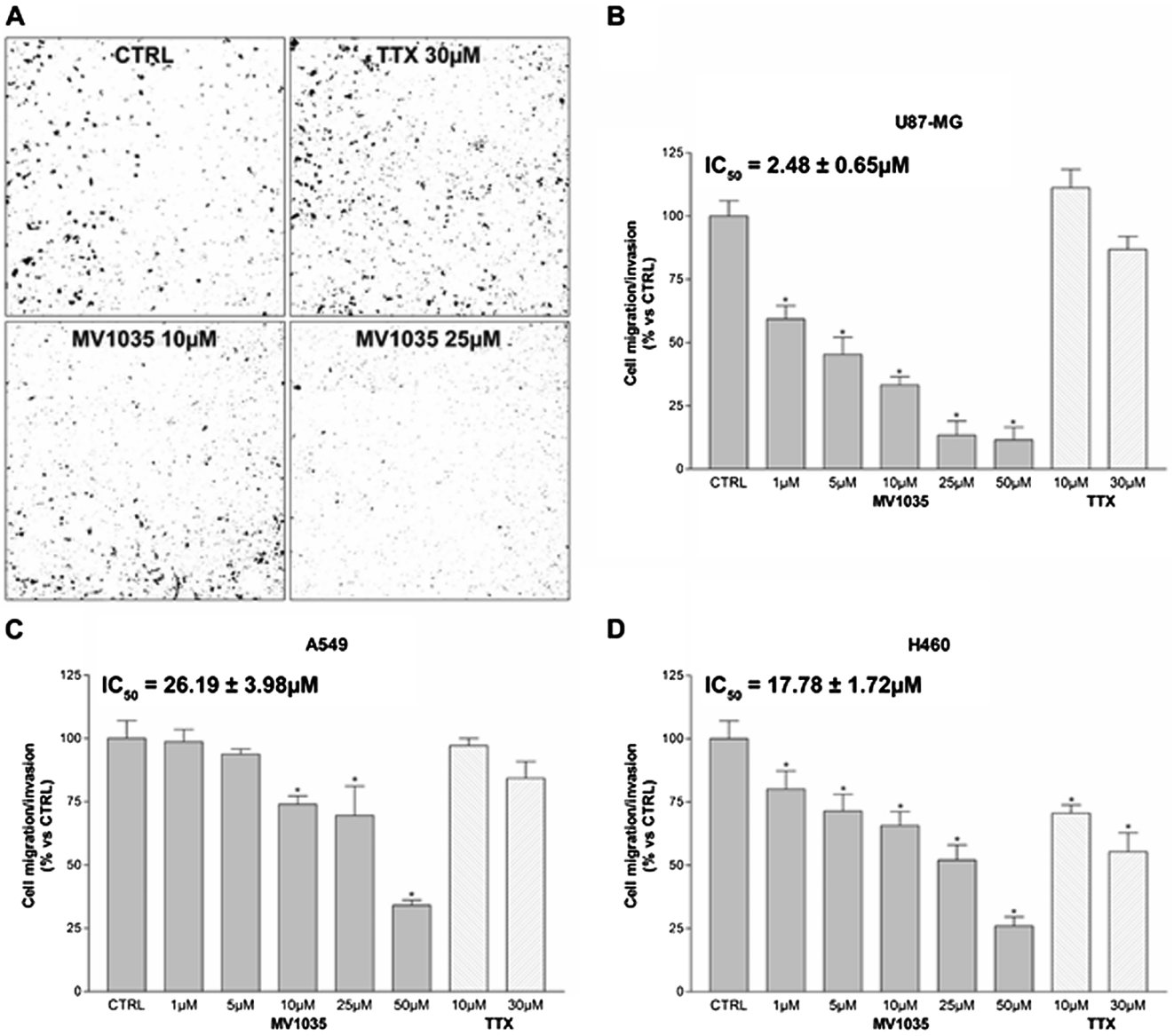

Fig. 3. Invasiveness of cells treated with MV1035 and TTX – Representative images of Boyden chamber assay of U87-MG cells not-treated (CTRL) or treated with TTX 30 μM or MV1035 (10–25 μM) (A). Graphs represent U87-MG (B), A549 (C) and H460 (D) cell invasion quantification after treatment with increasing concentrations of MV1035 (1–50 μM) or TTX (10–30 μM). Data are represented as the average percentage ± SD of three independent experiments compared to untreated control cells (CTRL, 100%) (* $P < 0.05$ vs CTRL).

relative stabilizing contribution to the ligand binding is reported in Supplementary Table S1.

2.2.3. In silico screening and ranking of the protein database

A systematic and unbiased search for the MV1035 PBSs within all protein 3D-structures included in the database was carried out by SPILLO-PBSS. Calculations were performed using a rotation step of 30° and a grid spacing of 2.0 Å, with a geometric tolerance set to the default value of 5.5 Å. For each protein, a ranking of the PBSs for MV1035 was obtained and stored by the program. Finally, the whole protein database was ranked according to the highest PBS score, representing the highest similarity to the RBS, obtained from each analysed protein 3D-structure.

3. Results and discussion

3.1. Chemistry

2-Methyl-3-propyl-5H-imidazo[1,2-c][1,3]benzoxazin-5-thione (MV1035) was synthesized, isolated and characterized as previously described.[35,36]

3.2. Biological evaluation

3.2.1. Cytotoxicity assays

In order to evaluate MV1035 cytotoxicity effect on U87-MG, A549 and H460 cells MTT and SRB assays were performed.

Cells were treated for 24 h with increasing concentrations of MV1035 (1–50 μM). The effect of well-known voltage-gated sodium channels inhibitor, tetrodotoxin (TTX, 10–30 μM) was also evaluated as positive control. Untreated cells represented negative controls.

As shown in Fig. 1, MV1035 slightly impairs cell viability of A549 in a dose dependent manner while has no statistical significant effect on H460 and U87-MG cells viability. TTX treatment does not affect viability in all the cell lines evaluated, except for a 25% reduction observed when tested at 30 μM concentration on A549 and H460 cells in the SRB assay. These results were in line with what we expected regarding the effect of sodium channel blockers on cell viability.

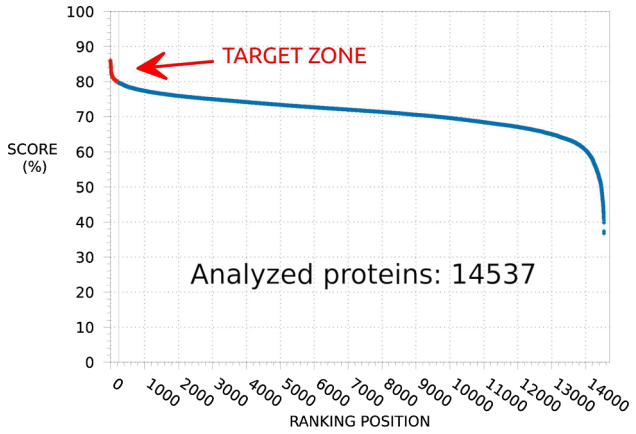

Fig. 4. SPILLO-PBSS screening and ranking of the available human structural proteome - Plot resulting from the *in silico* screening and ranking carried out by SPILLO-PBSS on the available human structural proteome (14537 protein 3D-structures retrieved from the RCSB Protein Data Bank in September 2017, excluding 100% sequence identity redundancies). Proteins are ranked in decreasing order according to their score. Potential target proteins of MV1035 show score values clearly higher than all others: they correspond to the 'target zone' (in red) on the left side of the line passing through the point of maximum upward concavity of the curve.

3.2.2. Migration test

Scratch wound healing assay was performed to evaluate the effect of MV1035 on cell migration of U87-MG, A549 and H460 cells. A scratch was caused on cell monolayer and cells were then treated for 24 h (6 h for U87-MG) with increasing concentrations of MV1035 (1–50 μM) or TTX (10–30 μM). Untreated cells represented controls.

MV1035 impairs cell migration of U87-MG and H460 cells in a dose dependent manner. On the contrary MV1035, only at 25 μM slightly increases A549 cellular migration.

10 μM TTX is not able to impair cell migration of all the cell lines considered. Contrariwise, 30 μM TTX increases the migration of U87-MG and A549 cells (Fig. 2).

3.2.3. Invasiveness test

In order to evaluate invasiveness of U87-MG, A549 and H460, Boyden chamber assay was performed. Cells were treated for 24 h with increasing concentrations of MV1035 (1–50 μM) or TTX (10–30 μM). Untreated cells represented controls.

MV1035 reduces invasiveness of U87-MG, A549 and H460 cells in a dose dependent manner. In particular MV1035 25 μM and 50 μM reduce U87-MG invasiveness by around 90%. On the contrary TTX is not able to reduce the invasiveness of U87-MG and A549 at both concentrations evaluated (10 and 30 μM). Instead, TTX impaired invasion ability of H460 cells in a dose dependent manner (Fig. 3).

These results were unexpected, in particular the effectiveness of MV1035 on migration and invasiveness of U87-MG cells seemed not related with its ability to block the sodium channels. This conclusion was supported by the fact that TTX was ineffective on U87-MG cells.

Considering the particular efficacy of MV1035 on glioblastoma migration and invasiveness and the crucial role of them on glioblastoma malignancy we have focused in depth molecular analysis on U87-MG cells.

3.3. SPILLO-PBSS screening

3.3.1. Protein database ranking

In order to identify a MV1035 target (different from Na_V) that could correlate to MV1035-induced reduction of U87 glioblastoma cells migration and invasiveness, we proceeded with the screening and ranking of the whole protein database carried out by SPILLO-PBSS. This analysis led to the non-linear plot reported in Fig. 4, whose points correspond to proteins ranked in decreasing order according to their scores. Interestingly, the non-linearity of the curve highlights the presence of a minority of proteins with scores clearly higher than all others, corresponding to the potential targets of MV1035.

3.3.2. ALKBH5 as potential off-target of MV1035

A first-level visual 3D-analysis of the 20 top ranked (out of 14537) potential targets of MV1035 was performed in order to classify the results into two different levels of accuracy: (i) likely true positives, and (ii) ambiguous hits. In particular, target proteins have been classified as likely true positives when the PBS identified by SPILLO-PBSS was located in a region corresponding to an already known binding site of the protein (e.g., because of the presence of another co-crystallized ligand), or in a region close to it. Unlike what happens with the traditional *in silico* techniques (e.g., molecular docking simulations), the results are considered acceptable even when they include steric clashes (see Supplementary Video S2 and the next paragraphs for more details). Instead, when the PBS fell in a protein region that was unlikely to be a binding site (e.g., because buried inside the protein), the proteins were classified as ambiguous hits. Based on this criteria, 13 of the 20 top

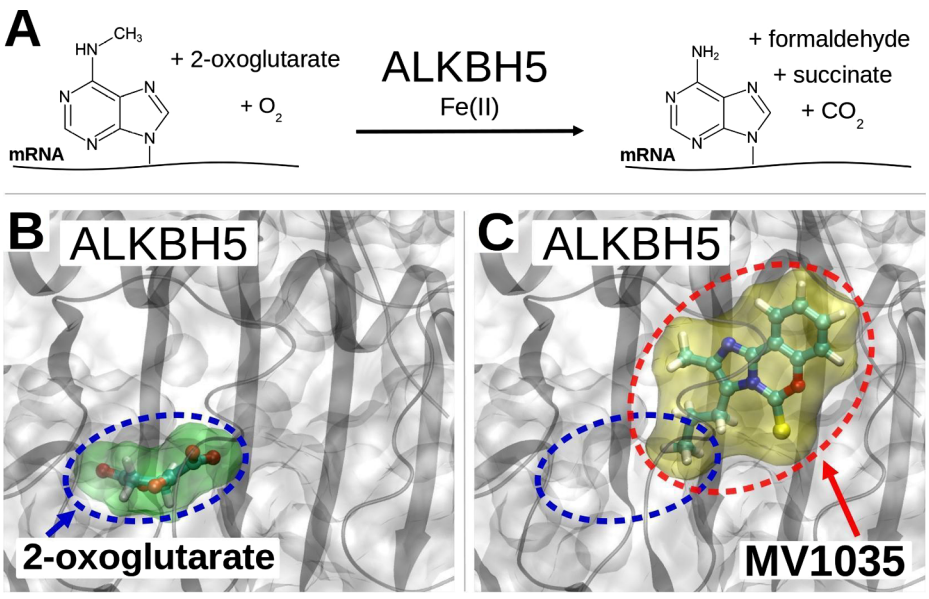

Fig. 5. ALKBH5 enzymatic reaction and competitive inhibition hypothesis. The enzymatic reaction (A) catalyzed by ALKBH5 is reported, along with the positions of 2-oxoglutarate (B) and MV1035 (C) within their corresponding binding sites, as obtained by x-ray diffraction (PDB code: 4oct) and SPILLO-PBSS calculation, respectively. The partial overlapping between the binding sites of 2-oxoglutarate and MV1035 is shown, which implies a competition between the two molecules for the same binding region, leading to the inhibition of the catalytic activity of the enzyme (drawings rendered using VMD[39,40]).

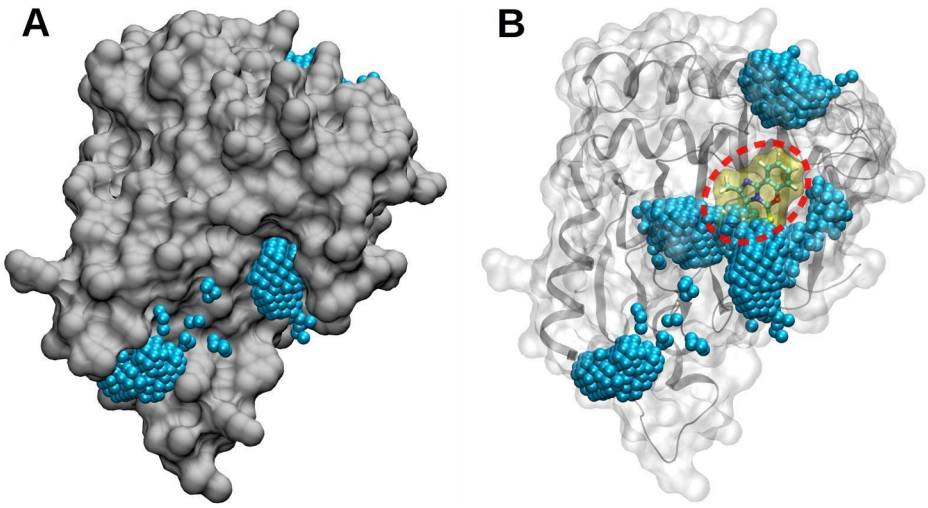

Fig. 6. The closed binding site for MV1035 identified by SPILLO-PBSS. The PBS for MV1035 (in yellow) identified by SPILLO-PBSS within the ALKBH5 protein crystal structure (PDB code: 4oct, chain A) is almost completely closed and buried inside the protein. Both surface (A) and cartoons (B) representations of ALKBH5 are provided. To make the closure of the binding site more perceptible, a visualization of the protein's cavities (as obtained by metaPocket 2.0[41,42] filled by probe spheres (in blue) is also provided, as opposed to semi-transparent regions, which represent parts of the protein occupied by protein's atoms. As can be noted, only a few atoms of MV1035 fall within a protein cavity, while the largest part of the molecule overlaps the atoms of the protein. The PBS identified by SPILLO-PBSS is apparently "inaccessible" and thus not detectable by traditional structure-based approaches (drawings rendered using VMD[39,40]).

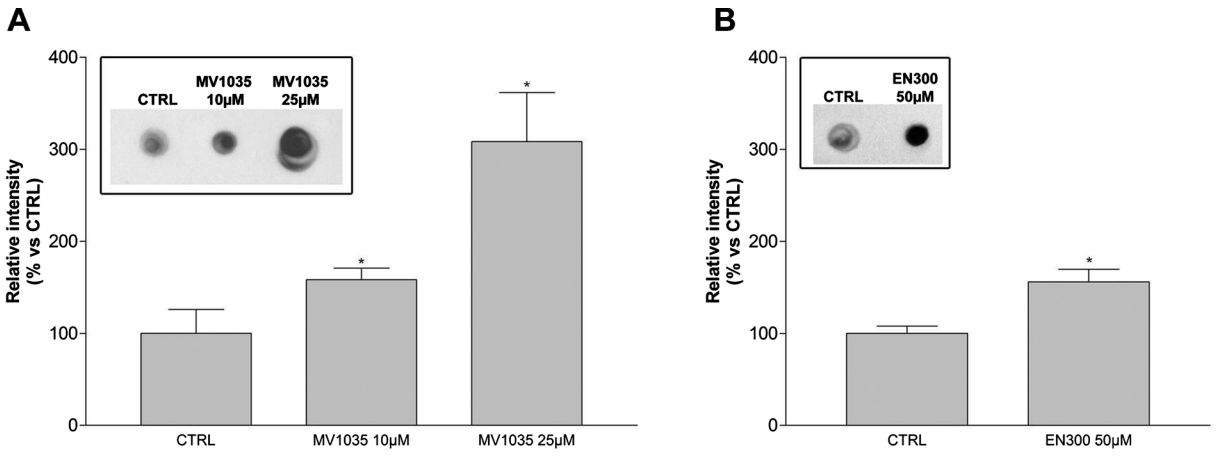

Fig. 7. Dot blot analysis of ALKBH5 demethylase activity - Dot blot analysis for the detection of m6A-RNA after the inhibition of ALKBH5 with MV1035 10 or 25 μM (A) or EN300 50 μM (B). The inserts show a representative image of m6A-RNA dot blot. Data are represented as the average percentage ± SD compared to controls without MV1035 or EN300 (CTRL, 100%). (* $p < 0.05$).

ranked proteins were classified as likely true positives.

After performing a literature search it emerged that 6 likely true positives were involved in cancer. In particular, we considered worthy of further investigation the RNA demethylase ALKBH5 enzyme (PDB code: 4oct). ALKBH5 catalyses the conversion of N6-methyladenosine (m6A) to adenosine in mRNA, in the presence of 2-oxoglutarate, molecular oxygen, and iron(II) (Fig. 5A)[28] and is involved in cancer and glioblastoma.[37,38] These findings pointed us towards ALKBH5 as important actor in MV1035-induced biological effect observed in U87 cells.

3.3.3. Competitive inhibition hypothesis

A potential binding site (PBS) for MV1035 was identified within the ALKBH5 3D-structure, which turned out to partially overlap with the catalytic site of the enzyme, specifically with the region occupied by the carboxylate group of 2-oxoglutarate. This allowed us to hypothesize an inhibition of the catalytic activity of the enzyme by MV1035 through the competition with 2-oxoglutarate for the same binding region (Fig. 5B and C).

3.3.4. SPILLO-PBSS ability in identifying closed binding sites

The identification of the ALKBH5 target protein was made possible by SPILLO-PBSS ability in recognizing PBSs independently on the particular conformation assumed by the protein (e.g., in the crystal structure). In fact, the novel PBS for MV1035 within ALKBH5 was identified despite its conformation that, in the analysed protein crystal structure, was almost completely closed and inaccessible to the molecule (Fig. 6). The innovative approach used by SPILLO-PBSS does not need the protein to be already in a suitable conformation for the binding. This allows SPILLO-PBSS to recognise putative binding sites that could not be found by traditional structure-based approaches (e.g., molecular docking simulations). For traditional methods atomic overlaps between the ligand and the protein are strongly forbidden, as they lead to extremely high repulsion energies and non-realistic situations. On the contrary, once SPILLO-PBSS recognizes a target binding site, even "inaccessible", it is possible to hypothesise that, under physiological conditions, both the protein and the ligand undergo local conformational rearrangements aimed at reproducing the stable situation represented by the RBS (see Supplementary Table S1 for a direct comparison between the MV1035 RBS and PBS).

3.4. Off-target validation

3.4.1. Dot blot

Dot blot analysis of methylated RNA was performed to evaluate the SPILLO-PBSS-predicted inhibition of active recombinant ALKBH5 by MV1035. ALKBH5 protein was mixed with m6A-RNA (CTRL) or with m6A-RNA and MV1035 (10 or 25 μM). Dot blotted methylated RNA significantly increases in a dose dependent manner in the presence of MV1035, reaching an increase of three fold compared to control

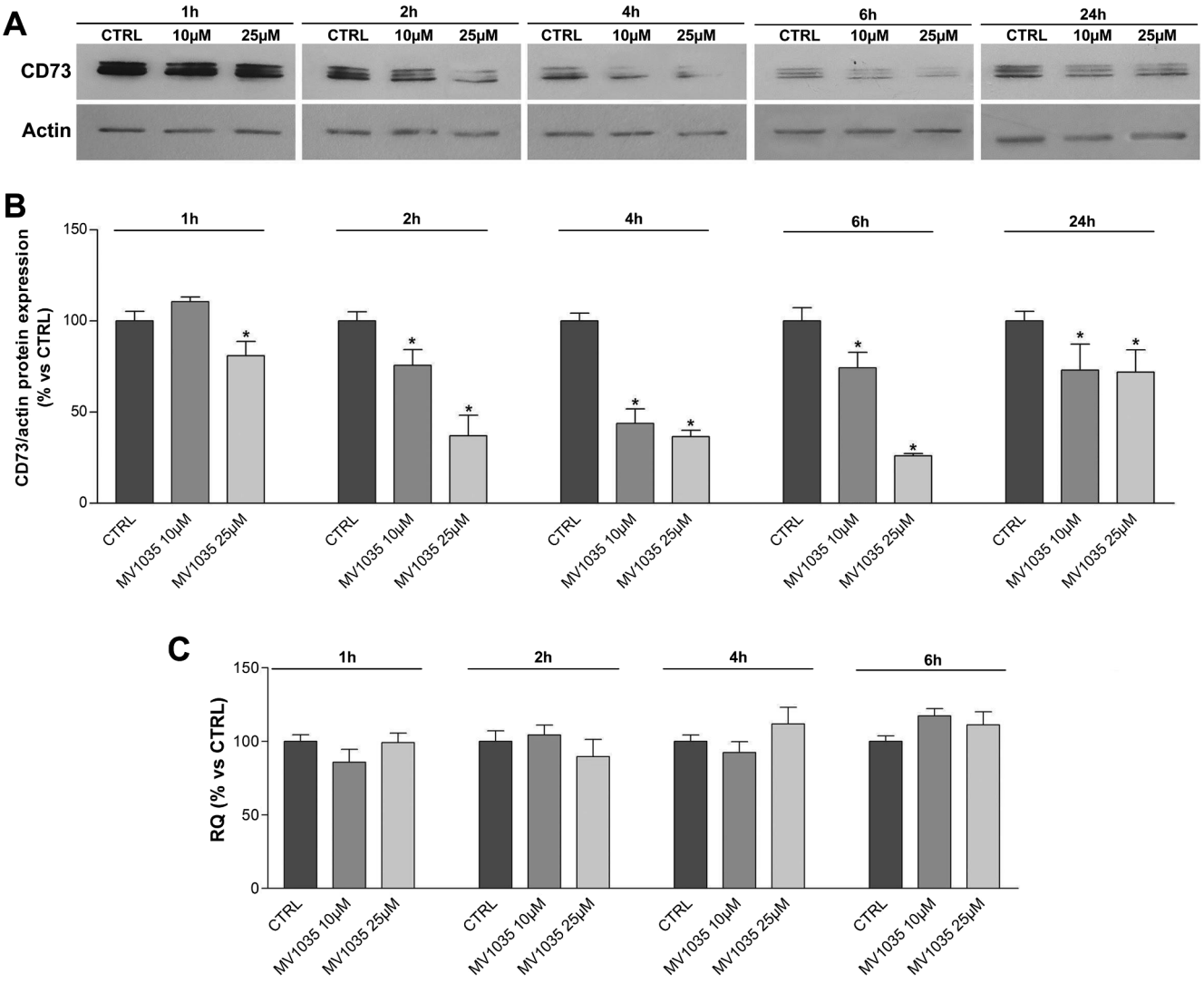

Fig. 8. Western blot and RT-PCR analysis in U87-MG cells. Representative images of CD73 western blotting (A) and respective graphs (B). Cells were treated for 1, 2, 4, 6 and 24 h with MV1035 10 or 25 μM. Graphs represent the average percentage ± SD of CD73 expression, normalized to actin and compared to untreated control cells (CTRL, 100%). (C) RT-PCR analysis of CD73 mRNA in U87-MG cells treated with MV1035 10 and 25 μM for 1, 2, 4 and 6 h. Data are represented as the average percentage ± SD compared to respective controls without MV1035 (CTRL, 100%).

(Fig. 7A).

EN300, a known inhibitor of ALKBH5, was used as positive control. As shown in Fig. 7B EN300 50 μM inhibits ALKBH5 and the level of methylated RNA is increased of 50% compared to the control.

These results confirmed the prediction made by SPILLO-PBSS that MV1035 is able to directly inhibit ALKBH5.

3.4.2. ALKBH5 and CD73

In order to evaluate the downstream effect of MV1035-induced ALKBH5 inhibition in U87-MG cells, CD73 protein expression was analysed. In fact, CD73 mRNA represents one of the main targets of ALKBH5 demethylase activity and its demethylation promotes CD73 protein expression.

U87-MG cells were treated with MV1035 10 or 25 μM. At different time points (1–24 h) total protein extracts were obtained and anti-CD73 immunoblotting analysis was performed (Fig. 8A). As shown in Fig. 8B, MV1035 reduces CD73 protein expression in a dose dependent manner. 10 μM MV1035 significantly reduces CD73 starting from 2 h of treatment, while the 25 μM MV1035 is already effective after 1 h of treatment.

In order to exclude that the CD73 protein expression reduction could be due to a MV1035-induced CD73 mRNA transcription decrease, CD73 RT-PCR was performed. Cells were treated for 1, 2, 4 and 6 h with MV1035 10 and 25 μM. As shown in Fig. 8C, MV1035 treatment does not induce a significant alterations of CD73 RNA levels compared to untreated controls.

These results as well as excluding any direct interaction between MV1035 and CD73 reinforced our theory that MV1035 targets preferentially ALKBH5 and this inhibition led to a downregulation of CD73 that could be useful in treating glioblastoma.

4. Conclusions

In the present work we show that MV1035, a compound based on the imidazobenzoxazin-5-thione scaffold, is able to reduce U87 GBM cells migration and invasiveness, targeting m6A demethylase ALKBH5. The strength of the data presented is due both to the crucial role in glioblastoma transformation of the identified MV1035 target but also to the innovative technique through which identification was made possible. In particular we used SPILLO-PBSS, a powerful software for identifying targets and off-targets of any small molecule on a proteome-wide scale, through an efficient identification of their binding sites. SPILLO-PBSS overcomes the traditional protein flexibility issue as it is able to identify the binding sites not only when they are in a suitable

conformation for the binding, like other software do, but also when they are strongly distorted, or even fully closed.

SPILLO-PBSS was able to point our attention on a pool of 20 possible targets. After a first-level visual 3D analysis 13 of them were classified as likely true positive; 6 of them turned out to be involved in cancer (from literature data).

Among the 6 likely true positive proteins involved in cancer we investigated m^6A demethylase ALKBH5 considering its crucial role in maintaining the tumorigenicity of glioblastoma stem like cells.[30] In fact evidence is growing regarding the role of m^6A methylation state in gene regulation.[44–46] There are many data underlying the correlation between this post translational modification and cancer.[29,47] In particular m^6A RNA methylation influences RNA stability, translational efficiency, secondary structure, subcellular localization and splicing.[44] Moreover aberrant expression of writers, erasers and readers of m6A methylation have been evidenced in tumorigenesis.[37] In particular ALKBH5 overexpression has been demonstrated in glioblastoma[38] and in breast cancer cells.[48] Noteworthy, SPILLO-PBSS showed how MV1035 binding site within ALKBH5 partially overlaps with the binding site of 2-oxoglutarate [see Supplementary Video S2] which, in turn, is necessary for the demethylation reaction to take place. Therefore, we were able to hypothesize that MV1035, competing with the substrates of ALKBH5, could inhibit the catalytic activity of this enzyme.

Biological evaluation performed in different cancer cell lines confirmed our hypothesis underlying that the MV1035 anti migration and anti invasiveness effect is independent from its ability to bind to sodium channels.

The compound was in fact originally tested trying to inhibit sodium channels in different cancer cell lines (with different Na_V expression profiles), following the rationale that blocking these channels in Na_v overexpressing tumors, usually leads to a remarkable decrease of their aggressiveness.[15,43] Experimental evidence, and the fact that TTX, a reference sodium channel blocker, showed no effect on migration and invasiveness of U87 cell line led us to hypothesize that MV1035 effectiveness could be based on a different mechanism of action.

We were then able to demonstrate that MV1035 directly inhibits active recombinant ALKBH5 protein and, consequently, negatively regulates CD73 protein expression without affecting CD73 mRNA transcription.

The results obtained are even more interesting considering the downregulation of CD73 expression. In fact, CD73 overexpression has been demonstrated in several cancer cell lines and tumor biopsies.[33,49] Moreover, CD73 is co-overexpressed in GBM with Multiple drug protein-1 (Mrp1). Quezada et al. have demonstrated that in GBM, inhibiting CD73 activity or knocking down CD73 expression, vincristine resistance is reversed through the reduction of Mrp1 expression.[50] Moreover among the different mechanisms that regulate CD73 expression there are also epigenetic modifications and in particular CpG island methylation has been correlated with several cancers.[51–53]

In this context, as further studies, it would be interesting to investigate the possible MV1035-induced modulation of Mrp1 and the effect of this compound as co-treatment with antineoplastic drugs for which GBM shows a high resistance. It is in fact also true that the effect of the methylating agent temozolomide, the golden standard for GBM treatment, is limited by chemoresistance, principally due to ATP binding cassette (ABC) transporters to which Mrp1 belongs.[54]

In perspective, MV1035 could result even more interesting because another top target recognized by SPILLO-PBSS (currently under investigation) is the DNA repair protein AlkB homolog 2 (ALKBH2), abundantly expressed in GBM cell lines, and demonstrated to be responsible for temozolomide resistance.[55] If so MV1035 could act on multiple targets belonging to the same disease-relevant target network both by inhibiting GBM migration and invasiveness and inactivating DNA repair mechanisms that concur to GBM resistance to temozolomide.

The described results, besides being important for studying glioblastoma molecular pathways and for developing new antineoplastic strategies, allowed us to identify a brand new ALKBH5 inhibitor. Furthermore they bring an additional value as we were able to validate experimentally SPILLO-PBSS *in silico* prediction.

Declaration of Competing Interests

The authors declare that they have no known competing financial interests or personal relationships that could have appeared to influence the work reported in this paper.

Appendix A. Supplementary material

Supplementary data to this article can be found online at https://doi.org/10.1016/j.bmc.2019.115300.

References

1. Daniel P, Sabri S, Chaddad A, et al. Temozolomide induced hypermutation in glioma: evolutionary mechanisms and therapeutic opportunities. *Front Oncol.* 2019;9:41. https://doi.org/10.3389/fonc.2019.00041.
2. van Tellingen O, Yetkin-Arik B, de Gooijer MC, Wesseling P, Wurdinger T, de Vries HE. Overcoming the blood–brain tumor barrier for effective glioblastoma treatment. *Drug Resist Updat.* 2015;19:1–12. https://doi.org/10.1016/j.drup.2015.02.002.
3. Raucher D, Dragojevic S, Ryu J. Macromolecular drug carriers for targeted glioblastoma therapy: preclinical studies, challenges, and future perspectives. *Front Oncol.* 2018;8:624. https://doi.org/10.3389/fonc.2018.00624.
4. Balça-Silva J, Matias D, do Carmo A, Sarmento-Ribeiro AB, Lopes MC, Moura-Neto V. Cellular and molecular mechanisms of glioblastoma malignancy: implications in resistance and therapeutic strategies. *Semin Cancer Biol.* 2018. https://doi.org/10.1016/j.semcancer.2018.09.007.
5. Jue TR, McDonald KL. The challenges associated with molecular targeted therapies for glioblastoma. *J Neurooncol.* 2016;127:427–434. https://doi.org/10.1007/s11060-016-2080-6.
6. Witthayanuwat S, Pesee M, Supaadirek C, Supakalin N, Thamronganantasakul K, Krusun S. Survival analysis of glioblastoma multiforme. *Asian Pac J Cancer Prev.* 2018;19:2613–2617. https://doi.org/10.22034/APJCP.2018.19.9.2613.
7. Besson P, Driffort V, Bon É, Gradek F, Chevalier S, Roger S. How do voltage-gated sodium channels enhance migration and invasiveness in cancer cells? *Biochim Biophys Acta.* 2015;1848:2493–2501. https://doi.org/10.1016/j.bbamem.2015.04.013.
8. Patel F, Brackenbury WJ. Dual roles of voltage-gated sodium channels in development and cancer. *Int J Dev Biol.* 2015;59:357–366. https://doi.org/10.1387/ijdb.150171wb.
9. Roger S, Gillet L, Le Guennec J-Y, Besson P. Voltage-gated sodium channels and cancer: is excitability their primary role? *Front Pharmacol.* 2015;6:152. https://doi.org/10.3389/fphar.2015.00152.
10. Black JA, Liu S, Waxman SG. Sodium channel activity modulates multiple functions in microglia. *Glia.* 2009;57:1072–1081. https://doi.org/10.1002/glia.20830.
11. Kis-Toth K, Hajdu P, Bacskai I, et al. Voltage-gated sodium channel Nav1.7 maintains the membrane potential and regulates the activation and chemokine-induced migration of a monocyte-derived dendritic cell subset. *J Immunol.* 2011;187:1273–1280. https://doi.org/10.4049/jimmunol.1003345.
12. Zuliani V, Patel MK, Fantini M, Rivara M. Recent advances in the medicinal chemistry of sodium channel blockers and their therapeutic potential. *Curr Top Med Chem.* 2009;9:396–415http://www.ncbi.nlm.nih.gov/pubmed/19442209.
13. Roger S, Rollin J, Barascu A, et al. Voltage-gated sodium channels potentiate the invasive capacities of human non-small-cell lung cancer cell lines. *Int J Biochem Cell Biol.* 2007;39:774–786. https://doi.org/10.1016/j.biocel.2006.12.007.
14. Fraser SP, Hemsley F, Djamgoz MBA. Caffeic acid phenethyl ester: Inhibition of metastatic cell behaviours via voltage-gated sodium channel in human breast cancer *in vitro*. *Int J Biochem Cell Biol.* 2016;71:111–118. https://doi.org/10.1016/j.biocel.2015.12.012.
15. Xia J, Huang N, Huang H, et al. Voltage-gated sodium channel Na $_v$ 1.7 promotes gastric cancer progression through MACC1-mediated upregulation of NHE1. *Int J Cancer.* 2016;139:2553–2569. https://doi.org/10.1002/ijc.30381.
16. Lopez-Charcas O, Espinosa AM, Alfaro A, et al. The invasiveness of human cervical cancer associated to the function of NaV1.6 channels is mediated by MMP-2 activity. *Sci Rep.* 2018;8:12995. https://doi.org/10.1038/s41598-018-31364-y.
17. Fulgenzi G, Graciotti L, Faronato M, et al. Human neoplastic mesothelial cells express voltage-gated sodium channels involved in cell motility. *Int J Biochem Cell Biol.* 2006;38:1146–1159. https://doi.org/10.1016/j.biocel.2005.12.003.
18. Vetter I, Mozar CA, Durek T, et al. Characterisation of Nav types endogenously expressed in human SH-SY5Y neuroblastoma cells. *Biochem Pharmacol.* 2012;83:1562–1571. https://doi.org/10.1016/j.bcp.2012.02.022.
19. Molenaar RJ. Ion channels in glioblastoma. *ISRN Neurol.* 2011;2011:590249. https://doi.org/10.5402/2011/590249.
20. Pollak J, Rai KG, Funk CC, et al. Ion channel expression patterns in glioblastoma stem cells with functional and therapeutic implications for malignancy. Ulasov I, ed. *PLoS*

ONE. 2017;12:e0172884. https://doi.org/10.1371/journal.pone.0172884.
21. Joshi AD, Parsons DW, Velculescu VE, Riggins GJ. Sodium ion channel mutations in glioblastoma patients correlate with shorter survival. *Mol Cancer.* 2011;10:17. https://doi.org/10.1186/1476-4598-10-17.
22. Schrey M, Codina C, Kraft R, et al. Molecular characterization of voltage-gated sodium channels in human gliomas. *NeuroReport.* 2002;13:2493–2498. https://doi.org/10.1097/00001756-200212200-00023.
23. Rivara M, Zuliani V, Patel MK. Biological evaluation of imidazobenzoxazines, imidazobenzoxazin-5-ones and imidazobenzoxazin-5-thiones as sodium channel blockers. *Lett drug Discov Des.* 2014:90–97.
24. Di Domizio A, Vitriolo A, Vistoli G, Pedretti A. SPILLO-PBSS: Detecting hidden binding sites within protein 3D-structures through a flexible structure-based approach. *J Comput Chem.* 2014;35:2005–2017. https://doi.org/10.1002/jcc.23714.
25. SPILLOproject. https://www.spilloproject.com.
26. RCSB Protein Data Bank. http://www.rcsb.org/.
27. Somody JC, MacKinnon SS, Windemuth A. Structural coverage of the proteome for pharmaceutical applications. *Drug Discov Today.* 2017;22:1792–1799. https://doi.org/10.1016/j.drudis.2017.08.004.
28. Xu C, Liu K, Tempel W, et al. Structures of human ALKBH5 demethylase reveal a unique binding mode for specific single-stranded N6-methyladenosine RNA demethylation. *J Biol Chem.* 2014;289:17299–17311. https://doi.org/10.1074/jbc.M114.550350.
29. Pan Y, Ma P, Liu Y, Li W, Shu Y. Multiple functions of m6A RNA methylation in cancer. *J Hematol Oncol.* 2018;11:48. https://doi.org/10.1186/s13045-018-0590-8.
30. Zhang S, Zhao BS, Zhou A, et al. m6A demethylase ALKBH5 maintains tumorigenicity of glioblastoma stem-like cells by sustaining FOXM1 expression and cell proliferation program. *Cancer Cell.* 2017;31:591–606.e6. https://doi.org/10.1016/j.ccell.2017.02.013.
31. Zhi X, Chen S, Zhou P, et al. RNA interference of ecto-5′-nucleotidase (CD73) inhibits human breast cancer cell growth and invasion. *Clin Exp Metast.* 2007;24:439–448. https://doi.org/10.1007/s10585-007-9081-y.
32. Morrone FB, Jacques-Silva MC, Horn AP, et al. Extracellular nucleotides and nucleosides induce proliferation and increase nucleoside transport in human glioma cell lines. *J Neurooncol.* 2003;64:211–218http://www.ncbi.nlm.nih.gov/pubmed/14558596.
33. Bavaresco L, Bernardi A, Braganhol E, et al. The role of ecto-5′-nucleotidase/CD73 in glioma cell line proliferation. *Mol Cell Biochem.* 2008;319:61–68. https://doi.org/10.1007/s11010-008-9877-3.
34. Azambuja JH, Gelsleichter NE, Beckenkamp LR, et al. CD73 downregulation decreases *In Vitro* and *In Vivo* glioblastoma growth. *Mol Neurobiol.* 2019;56:3260–3279. https://doi.org/10.1007/s12035-018-1240-4.
35. Fantini M, Zuliani V, Spotti MA, Rivara M. Microwave assisted efficient synthesis of imidazole-based privileged structures. *J Comb Chem.* 2010;12:181–185. https://doi.org/10.1021/cc900152y.
36. Rivara M, Fantini M, Acquotti D, Zuliani V. NMR analysis of a series of imidazobenzoxazines. *Magn Reson Chem.* 2010;48:500–503. https://doi.org/10.1002/mrc.2603.
37. Natalia P, Stephanie S, Justin J-LW. Aberrant expression of enzymes regulating m ^{6} A mRNA methylation: implication in cancer. *Cancer Biol Med.* 2018;15:323. https://doi.org/10.20892/j.issn.2095-3941.2018.0365.
38. Liu J, Ren D, Du Z, Wang H, Zhang H, Jin Y. m 6 A demethylase FTO facilitates tumor progression in lung squamous cell carcinoma by regulating MZF1 expression. *Biochem Biophys Res Commun.* 2018;502:456–464. https://doi.org/10.1016/j.bbrc.2018.05.175.
39. Humphrey W, Dalke A, Schulten K. VMD: visual molecular dynamics. p. 27–28 *J Mol Graph.* 1996;14:33–38http://www.ncbi.nlm.nih.gov/pubmed/8744570.
40. VMD - Visual Molecular Dynamics. http://www.ks.uiuc.edu/Research/vmd/.
41. Huang B. MetaPocket: a meta approach to improve protein ligand binding site prediction. *OMICS.* 2009;13:325–330. https://doi.org/10.1089/omi.2009.0045.
42. metaPocket 2.0. https://projects.biotec.tu-dresden.de/metapocket/index.php.
43. Campbell TM, Main MJ, Fitzgerald EM. Functional expression of the voltage-gated Na^{+}-channel Nav1.7 is necessary for EGF-mediated invasion in human non-small cell lung cancer cells. *J Cell Sci.* 2013;126:4939–4949. https://doi.org/10.1242/jcs.130013.
44. Fu Y, Dominissini D, Rechavi G, He C. Gene expression regulation mediated through reversible m6A RNA methylation. *Nat Rev Genet.* 2014;15:293–306. https://doi.org/10.1038/nrg3724.
45. Mauer J, Jaffrey SR. FTO, m6 Am, and the hypothesis of reversible epitranscriptomic mRNA modifications. *FEBS Lett.* 2018;592:2012–2022. https://doi.org/10.1002/1873-3468.13092.
46. Rajecka V, Skalicky T, Vanacova S. The role of RNA adenosine demethylases in the control of gene expression. *Biochim Biophys Acta - Gene Regul Mech.* 2019;1862:343–355. https://doi.org/10.1016/j.bbagrm.2018.12.001.
47. Tong J, Flavell RA, Li H-B. RNA m6A modification and its function in diseases. *Front Med.* 2018;12:481–489. https://doi.org/10.1007/s11684-018-0654-8.
48. Zhang C, Samanta D, Lu H, et al. Hypoxia induces the breast cancer stem cell phenotype by HIF-dependent and ALKBH5-mediated m ^{6} A-demethylation of NANOG mRNA. *Proc Natl Acad Sci.* 2016;113:E2047–E2056. https://doi.org/10.1073/pnas.1602883113.
49. Gao Z, Dong K, Zhang H. The roles of CD73 in cancer. *Biomed Res Int.* 2014;2014:460654. https://doi.org/10.1155/2014/460654.
50. Quezada C, Garrido W, Oyarzún C, et al. 5'-ectonucleotidase mediates multiple-drug resistance in glioblastoma multiforme cells. *J Cell Physiol.* 2013;228:602–608. https://doi.org/10.1002/jcp.24168.
51. Lo Nigro C, Monteverde M, Lee S, et al. NT5E CpG island methylation is a favourable breast cancer biomarker. *Br J Cancer.* 2012;107:75–83. https://doi.org/10.1038/bjc.2012.212.
52. Wang H, Lee S, Nigro CLo, et al. NT5E (CD73) is epigenetically regulated in malignant melanoma and associated with metastatic site specificity. *Br J Cancer.* 2012;106:1446–1452. https://doi.org/10.1038/bjc.2012.95.
53. Vogt TJ, Gevensleben H, Dietrich J, et al. Detailed analysis of adenosine A2a receptor (*ADORA2A*) and CD73 (5′-nucleotidase, ecto, *NT5E*) methylation and gene expression in head and neck squamous cell carcinoma patients. *Oncoimmunology.* 2018;7:e1452579. https://doi.org/10.1080/2162402X.2018.1452579.
54. Tivnan A, Zakaria Z, O'Leary C, et al. Inhibition of multidrug resistance protein 1 (MRP1) improves chemotherapy drug response in primary and recurrent glioblastoma multiforme. *Front Neurosci.* 2015;9:218. https://doi.org/10.3389/fnins.2015.00218.
55. Johannessen T-CA, Prestegarden L, Grudic A, Hegi ME, Tysnes BB, Bjerkvig R. The DNA repair protein ALKBH2 mediates temozolomide resistance in human glioblastoma cells. *Neuro Oncol.* 2013;15:269–278. https://doi.org/10.1093/neuonc/nos301.
56. MakeMultimer. http://watcut.uwaterloo.ca/tools/makemultimer/index.